INVERTED MICELLAR INTERMEDIATES AND THE TRANSITIONS BETWEEN LAMELLAR, CUBIC, AND INVERTED HEXAGONAL LIPID PHASES.

I. Mechanism of the $L_\alpha \leftrightarrow H_{II}$ Phase Transitions

D. P. SIEGEL
Procter & Gamble Co., P.O. Box 39175, Cincinnati, Ohio 45247

ABSTRACT A model for the thermotropic transitions between lamellar (L_α) and inverted hexagonal (H_{II}) phases is developed. According to this model, the first structures to form during the $L_\alpha \rightarrow H_{II}$ transition are inverted micellar intermediates (IMI). The structure, formation rates, and half-lives of IMI ("lipidic particles") were described previously (3). IMI coalesce in the planes between apposed bilayers to form two types of H_{II} phase precursors. The first is a monolayer-encapsulated H_{II} tube (RMI), which forms via coalescence of IMI in pearl-string fashion. These structures have been proposed previously based on electron microscopic evidence (26). I show that if only RMI form, $L_\alpha \leftrightarrow H_{II}$ transitions cannot occur on observed time scales (faster than seconds). I propose that a second type of intermediate, a line defect (LD), forms as well. LD should form via IMI-IMI coalescence in significant numbers, and elongate rapidly into structures consisting of two apposed halves of H_{II} tubes. Transitions via LD can occur in less than seconds, the time depending on the fraction of IMI-IMI coalescence events producing LD and the number of IMI per unit of bilayer area. Hysteresis in the phase transition temperature may be due to the difference in water content of the two phases and their low water permeabilities. The model is in qualitative agreement with morphological, NMR, and x-ray diffraction data on phospholipid systems. The results are relevant to IMI-mediated interactions between unilamellar bilayer vesicles (3), and to the structure of inverted cubic phases observed in some phospolipid systems (23, 24). These will be discussed in subsequent publications (22, D. P. Siegel, manuscript in preparation).

INTRODUCTION

Nonbilayer structures, such as inverted micellar structures and the inverted hexagonal (H_{II}) phase, can form in many phospholipid and glycolipid systems. These structures and their possible relevance to biomembrane processes have been the object of extensive research (see references 1 and 2 for recent reviews), particularly in regard to membrane fusion and exocytosis (3 and references therein; 2, 4). Many biomembranes and membrane lipid extracts can adopt the inverted hexagonal (H_{II}) phase under some conditions (5–10). Theory (11) indicates that even phospholipid membranes with fairly large mole fractions of charged, non-H_{II}-forming lipid will adopt the H_{II} phase if the bilayers are closely enough apposed ("dehydrated"). Membranes containing lipids that can adopt the H_{II} phase can easily be closely apposed (12–15) and may undergo fusion via inverted micellar intermediates (2–4, 16). Such intermediates and the H_{II} phase itself are induced by interactions with agglutinins and some proteins (17–19), and some proteins bind to membranes more easily in the presence of these intermediates (20). The activity of some proteins may be modulated by the tendency of membranes to form nonbilayer structures (21). Nonbilayer structures may occur with significant frequency in biomembranes, and may affect the kinetics of many biological processes.

All of these structures are associated with the transition to the H_{II} phase. It is important to understand the structure and dynamics of intermediates in the $L_\alpha \rightarrow H_{II}$ transition in order to determine the effects of these structures on biomembrane behavior. Here, I discuss the types of intermediates that are likely to form, and make order of magnitude estimates of their numbers, half-lives, and the rate of the phase transition under certain circumstances. The implications of this model for the types and rates of membrane-membrane interactions in vesicle dispersions near the $L_\alpha \rightarrow H_{II}$ transition of the lipid will be discussed in Part II (22). Implications concerning the structure of the inverted cubic phase observed in some phospholipid systems (23, 24) will be discussed in Part III (D. P. Siegel, manuscript in preparation).

THEORY

Overview

The $L_\alpha \rightarrow H_{II}$ transition is viewed as a three-step process. First, IMI (3) form between apposed lipid bilayers (Fig.

1). IMI can diffuse in the plane between the apposed bilayers, and encounter other IMI. The second step is IMI coalescence (Fig. 2) and formation of H_{II} precursors (Figs. 3, 4). The rate of this process is modeled as a two-dimensional Smoluchowski aggregation rate multiplied by an activation energy term. The third step is alignment of the precursors into bundles of H_{II} tubes (Fig. 5).

The second step, IMI coalescence, can produce two types of structures. IMI can coalesce in pearl-string fashion to form rod micellar intermediates (RMI, Fig. 3), which are essentially H_{II} tubes sandwiched between the two original bilayers. This mechanism has been proposed previously (e.g., 25, 26) on the basis of freeze-fracture electron microscopy data (e.g., 1, 25–27). Growth of RMI by successive coalescence events is slow.

I propose that IMI coalescence can also result in the formation of a second structure; a line defect (LD, Fig. 4). The structure that is the immediate consequence of IMI coalesence (Fig. 4, top) is two spherical micelles enveloped by an exterior monolayer. This structure can evolve into either an RMI or an LD. If the spherical micelles diffuse far enough apart, the two thicknesses of exterior monolayer neck down between them, and form a region that resembles the walls of two adjoining H_{II} tubes in cross section (Fig. 4, bottom). The geometry of this region is very similar to the H_{II} phase, and it can accrue lipid from the contiguous bilayer regions by diffusion. LD elongate and incorporate lipid into the H_{II} phase rapidly. Morphology consistent with LD structure has been observed (1, 23, 25, 28). LD and RMI produce H_{II} tubes lying in the planes of the original bilayers, which is the alignment of the two phases that is observed (6, 30, 31).

The third step in the transition is the sideways aggregation of LD and RMI into arrays of H_{II} tubes (Fig. 5). The difference of the RMI, LD, and H_{II} tubes with respect to the inter-bilayer spacing in the L_α phase results in smaller van der Waals attractive forces between bilayers containing them. This drives lateral phase-separation of the RMI and LD into bundles of H_{II} tubes. In the case of LD, sideways aggregation is also driven by LD elongation: uptake of bilayer lipid into two separated LD tends to draw them together in the plane of the bilayers. This process is also visible in electron micrographs (23).

I will explicate each of these steps below and then derive estimates of the kinetics of $L_\alpha \leftrightarrow H_{II}$ phase transitions.

Role and Formation of IMI

IMI are inverted micelle-containing structures that form between closely apposed bilayers. A cross-sectional view of an IMI is given in Fig. 1. Morphology consistent with this structure has been observed in many systems, and is the first evidence of the phase transition when the transition is approached by either changes in temperature or in in lipid composition (1; 3 and references therein). Expressions for the formation rate and half-lives of IMI were derived in

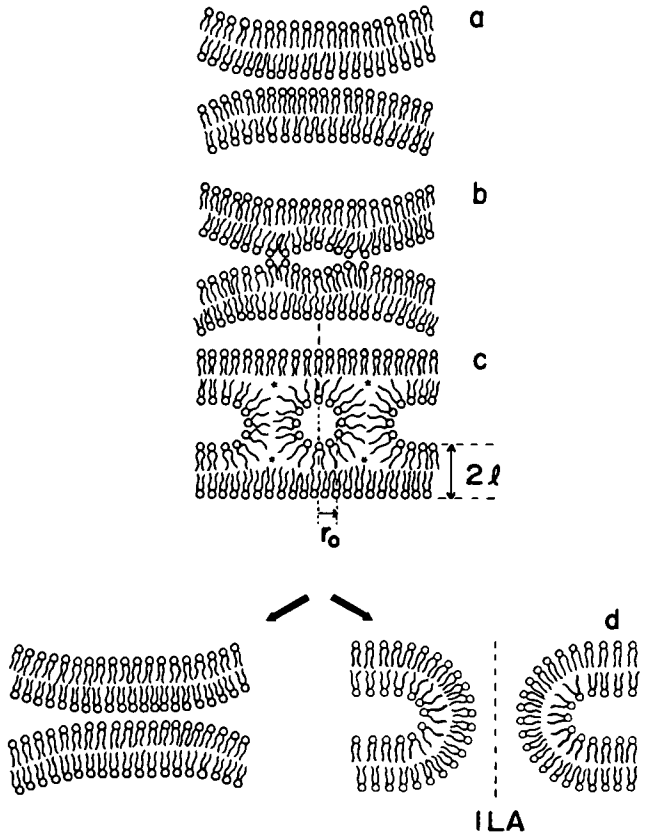

FIGURE 1 Formation of an IMI. Two bilayers (*a*) are closely apposed (*b*). The interfaces merge at the periphery of a circular patch of lipid to form the IMI (*c*). The IMI is cylindrically symmetrical about the vertical axis. The inverted micelle in the center is spherical. The IMI can revert to either of two bilayer structures (*d*); the original patch of apposed bilayers (*left*); or (rarely) to an interlamellar attachment (ILA, *right*). The ILA is also cylindrically symmetrical about the vertical axis, and makes the two original bilayers continuous.

reference 3. Some refinements to the method in reference 3 are described here.

In reference 3, IMI formation was treated as a three-step process. I will summarize them, as the same principles are applied in this work. First, the bilayers have to be closely-enough apposed (to within <1 nm) for the motions of molecules in the interfaces to become correlated. This will happen infrequently in most systems, due to the short-range repulsive forces between bilayers (31–33). Second, the local lipid concentration in the patch of closely apposed membranes must be sufficient for IMI formation: this is almost always true (3). Finally, the lipids rearrange into the IMI structure.

The influence of the close-apposition step on the IMI formation rate can be treated as a stationary probability of close-apposition, P_a;

$$P_a = \exp(-G_{app}/kT), \quad (1)$$

where G_{app} is the free energy required to appose the interfaces to within <1 nm. G_{app} can be estimated from interlamellar force measurements (31–33). Rearrange-

ment of the bilayer patches into IMI probably occurs as shown in Fig. 1. The lipids on the periphery of a patch of apposed bilayer interfaces containing the number of molecules that will form the inverted micelle become closely apposed (Fig. 1 *b*). When pressed closely together on this locus, the interfaces merge to form the inverted micelle and the external semi-toroidal monolayer of the IMI (Fig. 1 *c*). The IMI formation rate is described in terms of an Arrhenius rate constant. The frequency factor is the lipid chain rotational isomerization rate, α_1. This is so because the major difference between the conformation of a lipid molecule in the H_{II} and L_α phases is the increased disorder and projected area of the alkyl chains (11, 34). This time scale is also roughly the lipid molecule displacement time scale (the rate at which molecules can rearrange into new order). Increases in the number of kinks in the acyl chains must be tightly coupled to lateral displacements of lipid molecules in the bilayer. This time scale is ~10 ns (34–36), and $\alpha_1 \approx 10^8$/s.

The activation energy for rearrangement into IMI structure, $G^\ddagger$ is composed of two terms (3). The first is G_{mic}, the energy required to make the two interfaces continuous, and is given by

$$G_{mic} = (2\pi n_m)^{1/2} E = (8\pi^2 r_0^2/a_0)^{1/2} E, \qquad (2)$$

where E is the activation energy per lipid molecule for this process, a_0 is the area per lipid molecule at the lipid-water interface in the H_{II} phase. r_0 is the radius of the water cavity of the inverted micelle, and can be calculated from the dimensions of the L_α and H_{II} phases (3; and Eq. 6, below).

We can only guess at E, and merely offer a rationale for the value used in reference 3. Near the $L_\alpha \rightarrow H_{II}$ transition, the major contribution to E will be the energy necessary to simultaneously disrupt head group-head group interactions within the monolayer planes and form them between lipids on the apposed interfaces. Given the similar environment of lipids in the IMI to that of the H_{II} phase and the trivial chemical potential difference $\Delta\mu$ between the H_{II} and L_α phases at the transition temperature (3), it is likely that the changes in acyl chain conformation and head group area are almost spontaneous. The energy of head group-head group interactions is probably about a couple of kT (e.g., hydrogen bond energies in lipids like phosphatidylethanolamine), and such interactions exist between given head groups only a fraction of the time. Moreover, new interactions will be developing as old ones end. Hence, we assume that E is about $kT/2$, as in reference 3.

The second component in $G^\ddagger$ is G_{def}, the free energy of activation that accounts for the nonequilibrium radius of curvature of the exterior monolayer of the IMI. We can make a more accurate estimate of G_{def} than in reference 3 as follows.

The exterior surface of the IMI has two principal radii of curvature. The first is negative in sign and swings in the plane normal to the apposed bilayers. The second is of opposite sign, and swings in the plane parallel to the apposed bilayers. The sign of the radius indicates the sense of curvature; i.e., positive curvature corresponds to head groups splayed apart (head groups farthest from the origin), negative to head groups pressed together (head groups closest to the origin). The first of these principle radii has the same negative sign and about the same magnitude as the equilibrium H_{II} water channel radius, r_h. The second, however, is of positive sign: the head groups are splayed apart, exposing some hydrophobic moieties to the aqueous phase, which is energetically unfavorable.

However, the curvature free energy of this surface should be small because of its compound curvature. This reflects the compensatory nature of the two lipid packing schemes represented by the two principal radii of curvature of the surface: the head groups are splayed apart (small positive radius of curvature) in the plane parallel to the bilayers, but are packed more closely in the plane normal to the bilayers (small negative radius of curvature). This can be demonstrated using Helfrich's expression (37) for the curvature elastic free energy of interfaces. At and above T_H, $-r_h$ is the equilibrium radius of curvature, and

$$G_{def} = Sk_c(1/R_{av} - 1/r_s + 1/r_h)^2. \qquad (3)$$

S is the surface area of the external lipid-water interface of an IMI (3),

$$S = 2\pi^2 r_s(r_0 + r_s + 2l) - 4\pi r_s^2, \qquad (4)$$

where l is the thickness of a lipid monolayer (assumed to have the same value in the L_α and H_{II} phase). k_c is the bending elastic modulus of the interface, R_{av} the average positive radius of curvature of the external monolayer, and r_s the negative radius of curvature. r_h is negative, and $r_s \approx r_0$ (3). k_c for monolayer interfaces cannot be evaluated directly, although bilayer values are 10^{-13} to 10^{-12} ergs (38, 39). It can be shown that the inverse of the area-average positive radius of curvature $1/R_{av}$ on surface S, R_{av}, is given by

$$1/R_{av} = 2\pi^2 r_s/S. \qquad (5)$$

Equations like Eq. 3 have been used (11) to describe the free energy of lipid molecules in the H_{II} phase, which is similar to this structure. In IMI, R_{av} is typically about four times larger than the magnitude of r_s. Small (30%) reductions in r_s relative to r_h are sufficient to reduce G_{def} to zero. In fact, the value of r_s that makes G_{def} much less than kT for egg PE is also r_0, the value corresponding to most rapid IMI formation (Eq. 8, below). Therefore, G_{def} should be less than kT for most systems.

Kirk, Gruner, and Stein (11) pointed out that some acyl chains in the H_{II} phase must stretch out to fill the interstitial spaces between H_{II} rods. This reduces the conformational freedom of the chains, and makes a substantial contribution to the chemical potential difference between the L_α and H_{II} phases, $\Delta\mu$. Such void volumes

appear in IMI as well (stars in Fig. 1 *c*). Differences in the interstitial void size in IMI and the H_{II} phase could affect the chemical potential differences between H_{II} and IMI, and hence our estimates of $G^{\ddagger}$. However, Fig. 1 *c* represents an idealized geometry. The lipid-water interfaces in IMI and the H_{II} phase can distort slightly to reduce the void volume to different extents. In reality, we don't know the void volume accurately in either case, and can't calculate this contribution to the free energy. It might be a significant contribution to $G^{\ddagger}$.

When $2r_0$ is large compared to the thickness of the aqueous layers in the L_α phase, there may be another contribution to $G^{\ddagger}$; the work of increasing interbilayer separation. With expressions for the van der Waals energy in multibilayer systems (40), it can be shown that this term is $<2\ kT$ for most r_0.

The formation rates and half-lives of IMI are calculated as in reference 3. r_0, the radius of the water cavity in the inverted micelle of the IMI, is given by

$$r_0 = \{-B + [B^2 - 8Wl^2]^{1/2}\}/2W, \tag{6}$$

where

$$B = l(4 - \pi b); \quad b = (\bar{a}/a_0)^{1/2}; \quad W = 2 - b(\pi + b - 1).$$

$\bar{a}$ is the area per lipid head group in the bilayer. G_{mic} is calculated via Eqs. 2 and 6. The IMI formation rate per unit area of apposed bilayers per unit time is

$$N_3 = (\alpha_1/A) \exp(-G^{\ddagger}/kT) P_a. \tag{7}$$

A is the minimum area of a patch of apposed bilayers that can form an IMI,

$$A = 4\pi(r_0 + l)^2. \tag{8}$$

Typical values of N_3 lie in the range of 10^{11}–10^{15} IMI cm^{-2} s^{-1} (3).

Around T_H, IMI are in dynamic equilibrium with the bilayers from which they form (3). The rate of reversion of IMI to bilayer structure is

$$P_{-3} = \alpha_1 \exp(-G^{\ddagger}_{-}/kT) P_r, \tag{9}$$

and the half-life with respect to reversion is

$$t_{1/2} = (2P_{-3})^{-1}, \tag{10}$$

where $G^{\ddagger}_{-}$ is the activation energy for reversion. Since this is simply the reverse of the IMI formation process, when $T = T_H$, $G^{\ddagger}_{-}$ will be given by

$$G^{\ddagger}_{-} = G^{\ddagger} = G_{mic} + G_{def}. \tag{11}$$

When $T \neq T_H$, $G^{\ddagger}_{-}$ is affected by the chemical potential difference $\Delta\mu$. When H_{II} is the more stable phase at equilibrium, a greater activation energy will be required to force the IMI lipids into a bilayer conformation. Typical values of $t_{1/2}$ at $T \approx T_H$ are in the range of milliseconds (3).

P_r in Eq. 9 represents the probability that the IMI will become distorted enough to revert to bilayer structure. This factor was neglected in reference 3, but is probably small compared to unity, and substantially affects the IMI lifetime and number density (below). IMI revision requires that the IMI flatten in the direction normal to the bilayers in order to reform the bilayer interfaces. P_r is analogous to P_a (Eq. 1). It is hard to evaluate P_r, since we know little about hydration forces in spherical geometries. (There is reason to believe that they will be weaker than those acting between planar bilayers; 11.) Some energy also has to be expanded in changing the curvature of the exterior surfaces of the IMI during this process. The fact that G_{def} is $<kT$ implies that this latter contribution is negligible. Therefore, the free energy required to deform an IMI sufficiently for reversion to begin is less than G_{app}, and $P_r > P_a$.

Let n_I be the instantaneous two-dimensional concentration of IMI. If the only IMI-consuming process is reversion,

$$dn_I/dt = N_3(1 - n_I A) - n_I P_{-3} \tag{12}$$

and

$$n_I = \frac{1 - \exp(-Ct)}{A\{1 + (P_r/P_a) \exp[(G^{\ddagger} - G^{\ddagger})/kT]\}}$$
$$= n_I^0[1 - \exp(-Ct)], \tag{13}$$

where

$$C = \alpha_1[P_r \exp(-G^{\ddagger}_{-}/kT) + P_a \exp(-G^{\ddagger}/kT)]. \tag{14}$$

n_I^0 represents the steady-state concentration of IMI if reversion is the only IMI decay process. $n_I(t)$ becomes n_I^0 after a time $\approx 1/C$ after T is brought to T_H.

In reference 3 it was shown that an IMI can revert to either a patch of apposed planar bilayers or an interlamellar bilayer attachment (ILA), (Fig. 1*d*, right). It was assumed that reversion formed both structures with similar frequency. A more detailed treatment (22) shows that reversion to ILAs should be much less frequent than reversion to planar bilayers. This has a substantial effect on the predicated rate of IMI-mediated membrane-membrane fusion in lipid dispersions (22). ILA form too infrequently in PE to affect the value of n_I^0 (Eq. 13).

IMI Coalescence

IMI can diffuse within the plane between the two apposed bilayers. IMI encounter others and coalesce in some fraction of the encounters. There is only a small thermodynamic driving force for coalescence (an increase in the positive radius of curvature of the exterior monolayers of the coalesced IMI). IMI coalescence is almost irreversible because coalescence intermediates are rapidly converted into more kinetically stable structures (rod micellar intermediates and line defects;, see below). The IMI coales-

cence rate is a two-dimensional reaction rate (41). We can make an order-of-magnitude estimate of it as follows.

We model the diffusion of an IMI as diffusion of the inverted micelle within the enveloping monolayers of the two apposed bilayers and the exterior surface of the IMI (Fig. 1 *c*). This results in motion of the IMI as a whole. As the micelle moves, a force is exerted on the exterior surface of the IMI. In response, the exterior surface is also displaced within the plane of the apposed bilayers. Equivalent numbers of lipid molecules are swept up into the exterior surface of the IMI at its leading edge and returned to the bilayer at its trailing edge.

We approximate the IMI diffusion coefficient, D_{IMI}, as that of the spherical inverted micelle in a three-dimensional, viscous fluid. This is obviously an over-simplification. The hydrodynamics of particle motion will not be those found in an extended continuum, and the monolayers aren't continuous, isotropic fluids. We assign a viscosity $\eta = 1$ poise to the fluid sheets with which we model the monolayers, which is compatible with the diffusion coefficients of lipids and proteins in the L_α phase (42, 43). D_{IMI} is given by the Stokes-Einstein relation,

$$D_{IMI} = kT/6\pi\eta\,(r_0 + l). \tag{15}$$

Using $\bar{a}$ and a_0 data for egg PE as in reference 3, and an egg PE monolayer thickness of 1.6 nm (21), D_{IMI} is 7×10^{-9} cm^{2}s^{-1} near room temperature. This is one-third the diffusion coefficient in the L_α phase of proteins of about the same dimensions as the micelle (42).

The coalescence rate of IMI can be described as the chemical reaction rate between two identical reactants in a two-dimensional system. Torney and McConnell (41) showed that to a good approximation the rate constant is

$$k_I = 8\alpha D_{IMI} \tag{16}$$

when the proportion of encounters that are reactive, α, is <0.1 and the system is dilute (i.e., when $n_I^0 < 1/2A$). I will show below that α will be <0.01. Eq. 16 may be inappropriate when IMI are almost close-packed ($n_I^0 \approx 1/2A$, the maximum value possible; 3). A more appropriate form can be derived for that limit (D. P. Siegel, unpublished results). For the purpose of making order-of-magnitude predictions, however, Eq. 16 will suffice.

Calculation of the Reactivity, α

Two things must occur for two IMI (Fig. 2 *a*) to coalesce. First, the outer surfaces of the enveloping monolayers at the "waists" of the IMI must be closely apposed to within some distance H (Fig. 2 *b*). Then the monolayers can become continuous, as in formation of IMI from apposed bilayers (Fig. 2 *c*). r_0 and r_s are larger than H. Thinning the channel between IMI requires an activation energy G_H, accounting for changes in curvature and work done against hydration forces.

During this process, lipid on the walls of the channel can diffuse into the adjoining bilayers to relieve local stresses due to curvature changes. This reduces the first contribution to G_H: the work against hydration forces probably dominates. We can estimate an upper bound for this contribution. The sides of the channels must be apposed on a locus about two molecules wide in order for coalescence to occur. Half the area of this locus is $\approx 2r_0(2a_0^{1/2})$, and the hydration component of G_H is less than the work done in bringing two bilayers of this area to within a distance of H of one another. Using force constants from reference 31

$$G_H = 4r_0a_0^{1/2}E', \tag{17}$$

where

$$E' = -P_0\int_{2r_0}^{H} \exp\{-x/\lambda\}\,dx = P_0\lambda\,[e^{-H/\lambda} - e^{-2r_0/\lambda}]. \tag{18}$$

P_0 and λ are measured hydration force constants for the lipid system (e.g., 31).

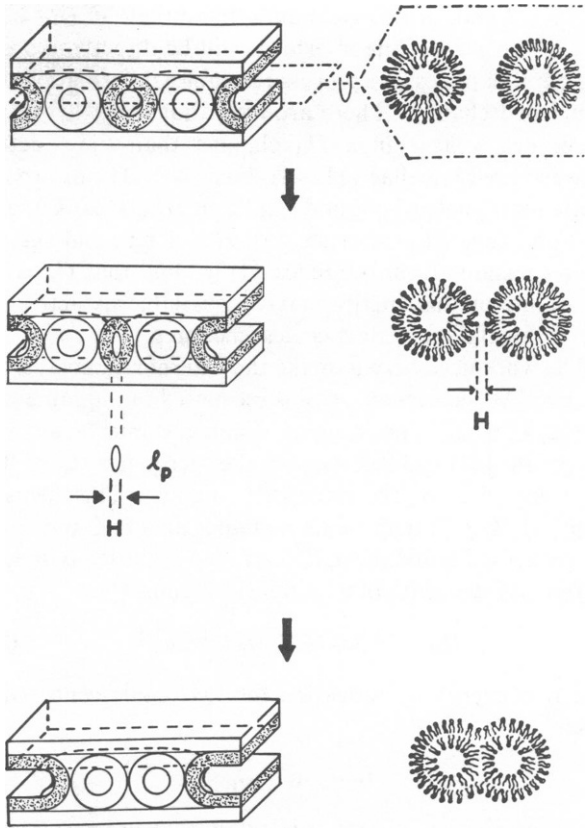

FIGURE 2 IMI coalescence. Two IMI, diffusing in the plane of the apposed bilayers (*top*) approach each other. The channel between the external monolayers thins by exchange of lipid with the continuous planar monolayers (*middle*). The channel reaches a thickness H at which the two monolayer walls can merge into a single interface. This produces (*bottom*) a coalescence intermediate (CI): the two spherical inverted micelles are enclosed by a single exterior monolayer. At the left, the monolayers are depicted as slabs. The edges of monolayers that are continuous (exterior monolayers of the two IMI and the facing monolayers of the bilayers) are shaded. The drawings on the right are cross-sections of the structures in the plane parallel to and equidistant from the bilayers (*top*).

Eqs. 17 and 18 will yield an over-estimate of G_H. Only part of the area of the interfaces will be directly apposed like parallel plates: the process resembles deformation of a cylindrical channel. There are indications that hydration forces are weaker in a H_{II} channel than those acting between lipid lamellae (11, 44). For r_0 = 1.34 nm (appropriate for dilinoleoyl-PE and egg PE at around 20°C), a_0 = 0.42 nm^2 (egg PE, reference 45), H = 1 nm, and egg PE force constants from reference 31, we find that G_H is <6 kT. Some of this energy may be available as activation energy for the succeeding coalescence step.

The work necessary to make the external monolayers of the two IMI continuous, G_M, is estimated in the same way as G_{mic} (Eq. 2). The locus at which the interfaces must merge in IMI coalescence is the perimeter l_p of the narrowest part of the inter-IMI channel. This locus is elliptical (Fig. 2; major axis r_0, minor axis H), and G_M is the product of E and the perimeter (46) of the locus divided by the average width of a lipid head group;

$$G_M \approx 2\pi[(r_0^2 + H^2)/2]^{1/2}E/a_0^{1/2}. \quad (19)$$

The free energy of activation for IMI coalescence G_I is given by

$$G_I < G_M + G_H. \quad (20)$$

α, the proportion of IMI encounters that are reactive, is simply

$$\alpha = \exp(-G_I/kT). \quad (21)$$

H_{II} PHASE FORMATION

IMI coalescence can produce either of two structures; rod micellar intermediates (RMI), or line defects (LD). Both these structures assemble into the H_{II} phase, but at different rates. The structure resulting from a given IMI coalescence event is determined by the competition of two processes: fusion of the two spherical inverted micelles within the coalescence intermediate into a single rod-shaped micelle (RMI, Fig. 3), and separation of the two micelles within the coalescence intermediate (leading to LD formation, Fig. 4).

RMI Formation

The initial product of IMI coalescence (the coalescence intermediate, or CI) is two spherical inverted micelles enveloped by the monolayers of the original IMI (Fig. 2 *c*). These can fuse into rod a micelle, forming an RMI. This process is visible in freeze-fracture electron micrographs: many authors (e.g., 1, 25–27) have published images of "lipidic particles" aggregating into or blebbing off from H_{II} tube structures.

In order to make two lipid-water interfaces continuous, they must be closely apposed to within some critical distance H. We assume that when two spherical micelles fuse, their interfaces first become continuous on a locus of this diameter H. The chemical potentials of lipid in rod and spherical micelles are almost identical near T_H. Thus, in analogy to IMI formation and IMI coalescence, the activation free energy for formation of the rod micelle will be the number of molecules on the locus at which the spherical

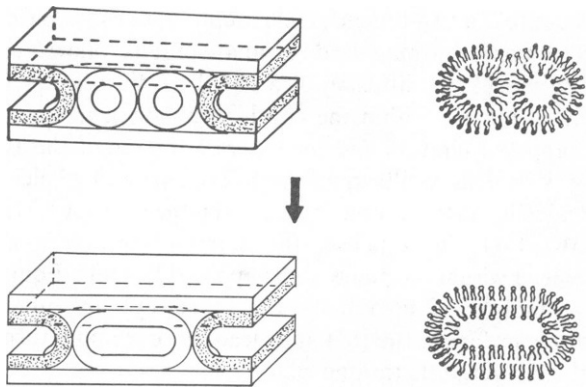

FIGURE 3 Fusion of two spherical micelles in a CI (*top*) to form a rod micellar intermediate, or RMI (*bottom*). The edges of the exterior monolayer of the CI are shaded, and the cross sections through the structures are depicted as in Fig. 2.

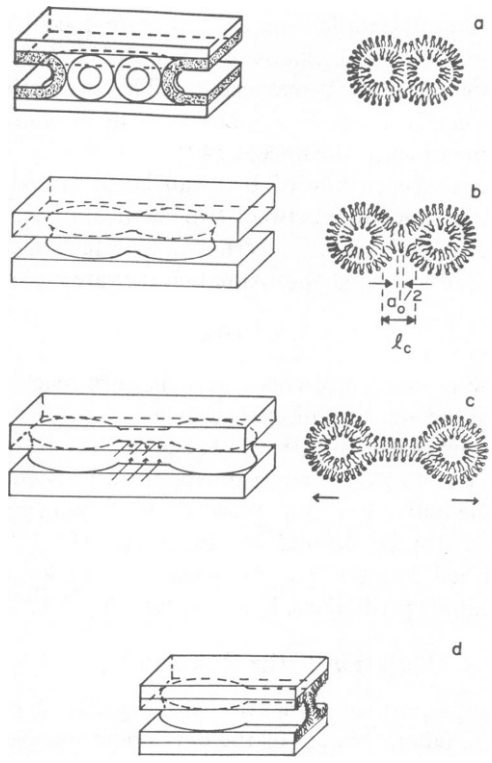

FIGURE 4 Formation of a line defect (LD) from a CI. The two spherical micelles on the CI (*a*) diffuse a distance l_c apart within the enveloping monolayer. The external monolayer necks down between them, forming an LD (*b*). A cross section of the region between the two micelles in the plane perpendicular to the apposed bilayers is shown in *d*: this region resembles the halves of two H_{II} tubes apposed with the hydrophobic surfaces in contact. Lipid molecules from the continuous planar bilayers diffuse directly into the H_{II}-like middle section of the LD (arrows in *c*), causing elongation of the LD (*right*-hand side of *c*).

micelle interfaces become continuous and an energy E. We assume that E has the same value as in IMI formation and coalescence. The rate of spherical micelle fusion is expressed as an Arrhenius rate constant with frequency factor α_1. In analogy to Eqs. 2 and 19, the activation energy for spherical micelle fusion into an RMI is

$$G_{RMI} = \pi HE/a_0^{1/2}, \quad (22)$$

and the rate of this process will be

$$k_{RMI} = \alpha_1 \exp(-G_{RMI}/kT). \quad (23)$$

These equations also give the rate of spherical micelle fusion with pre-existing rod micelles in CI (i.e., IMI coalescing with RMI terminals). Using $H = 1$ nm, $\alpha_1 = 10^8 s^{-1}$, and $E = kT/2$ as before, we find $k_{RMI} = 10^8 \exp(-3) \approx 10^6 - 10^7\ s^{-1}$ for egg PE: the half-life of the spherical micelles within CI is <1 μs.

Re-formation of spherical micelles from the rod micelles within RMI should be slower. In order to fission into two micelles, the diameter of the water channel in the rod micelle has to thin to a diameter H. This requires work against hydration and other forces, and an activation energy about equal to G_H (Eqs. 17, 18). The rate constant, k_S, for spherical micelle re-formation from an RMI at equilibrium rod micelle diameter is

$$k_S < \alpha_1 \exp\{-(G_{RMI} + G_H)/kT\} = k_{RMI} \exp\{-G_H/kT\}. \quad (24)$$

G_H (Eq. 17) can be as large as 6 kT, so k_S is much smaller than k_{RMI}. We therefore neglect the rate of rod micelle fission (CI re-formation from RMI) in our treatment of the $L_\alpha \rightarrow H_{II}$ transition.

RMI grow by repeated coalescence of IMI with the ends of the RMI. Coalescence of IMI with the sides of RMI is also possible. Since RMI have smaller diffusion coefficients and tend to align with sides parallel into the smallest area possible (see Assembly of LD or RMI into H_{II} Tubes, below), this may not be a frequent occurrence, however.

LD Formation

The spherical inverted micelles in the CI undergo Brownian motion within the exterior lipid monolayers. If the spherical micelles diffuse far enough apart before they fuse into a rod micelle, the exterior monolayers of the CI become apposed in the region between the separated micelles. In cross-section, this region resembles the walls of two adjoining H_{II} tubes (Fig. 4). The radius of curvature of the interfaces is r_h, and the chemical potential of lipid in this region is essentially that of H_{II} phase lipid. This region of the LD rapidly accrues lipid molecules from the adjoining bilayer by diffusion, and lengthens to accommodate the influx. This is a rapid, nearly zero activation-energy pathway between the L_α and H_{II} phases. It also automatically aligns LD and adjacent RMI into bundles of H_{II} tubes (Fig. 5).

Morphology consistent with LD structures (ripple pat-

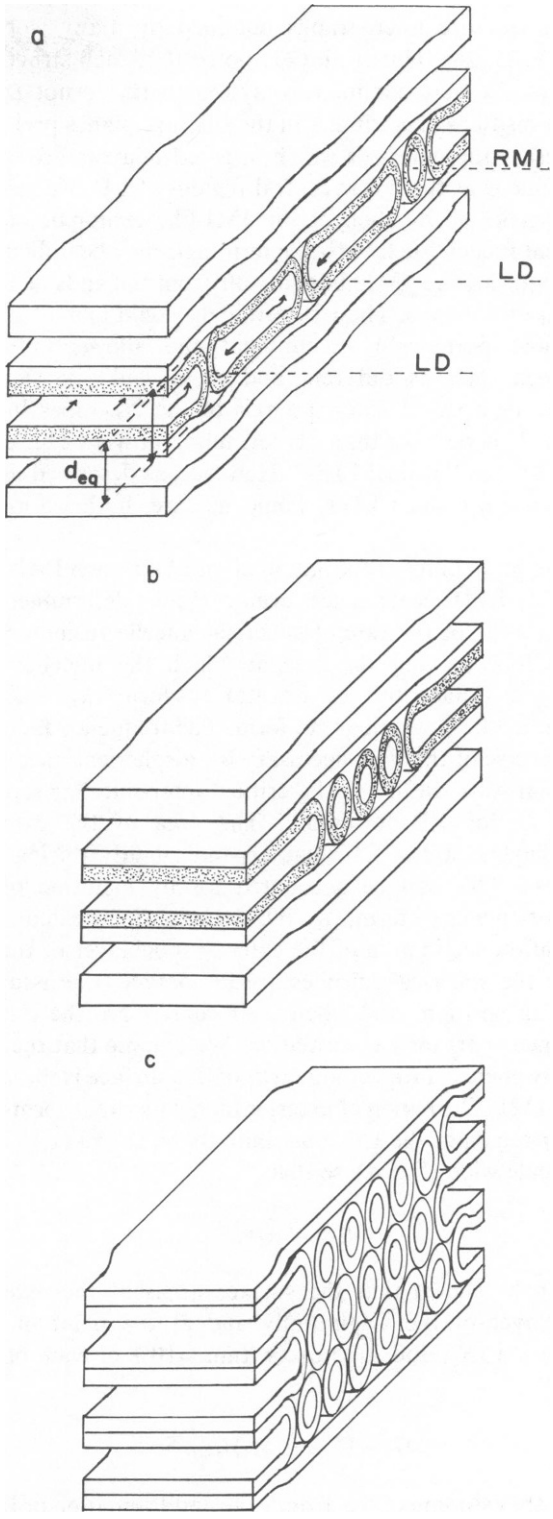

FIGURE 5 Assembly of LD and RMI into the bulk H_{II} phase. LD and RMI form between bilayers (*a*). Lipid diffusion into the LD (arrows) pulls the LD and RMI together (*b*) as the LD elongate (parallel to dotted lines in *a*). The diameters of LD, RMI, and H_{II} tubes are unequal to d_{eq}, and this alignment minimizes the area of the bilayer array with $d \neq d_{eq}$. LD and RMI formed between adjacent pairs of lamellae pack in the hexagonal scheme of the H_{II} phase to minimize the distance between H_{II} tubes (*c*).

terns that merge into H_{II} tube bundles) are visible in freeze-fracture micrographs obtained by many workers (1, 23, 25, 28). Hui et al. (23) noted that such structures ("ripples") were common for systems with abrupt $L_\alpha \leftrightarrow H_{II}$ transitions. The ripples in the fracture planes probably represent the points at which apposed bilayers are made continuous at the linear central regions of LD. Reports to date make no mention of the IMI-like terminals of the present model. Such IMI-like terminals may be difficult to distinguish from IMIs budding off from the ends of RMI in H_{II} tube arrays. The LD terminals would look like IMI ("lipidic particles") except that the allowed spacing between them is different and they would be slightly (~2nm) displaced from the axis of the H_{II} tubes in the array. It is possible that LD terminate in what Hui et al. have termed "conical LIPs." However, as described in the Discussion, conical LIPs should be rare, if they form at all.

The probability of formation of an LD in each IMI-IMI or IMI-RMI coalescence event, P_L, is determined by competition of the rate of spherical micelle fusion within the CI, k_{RMI}, and the rate at which the micelles can separate sufficiently for an LD to form, $k_L \cdot k_L$ is estimated in Arrhenius rate form. The frequency factor is the inverse of the time necessary for a spherical micelle to random-walk diffuse to the critical inter-micellar separation, l_c, for LD formation. The area of the exterior monolayers of the CI must expand slightly during this process. This can be accounted for by inclusion of an activation energy term, G_L. We estimate G_L by calculating the difference in area of the exterior monolayer of the CI when the spherical micelles are in contact (the assumed starting position) and when their centers are the critical distance apart for LD formation. We assume that the free energy of curvature per unit area of this surface is the same as in IMI. The region of exterior monolayer that forms the linear region of the LD must initially be at least one lipid molecule wide (Fig. 4), so that

$$l_c = 2l + a_0^{1/2}. \tag{25}$$

It can be shown that the surface areas of the exterior monolayer of the CI initially and at the point of LD formation (S_{CI} and S_{LD}) are within ~10% of each other. Since

$$G_L = (S_{LD} - S_{CI})G_{def}/S, \tag{26}$$

using the estimate of G_{def} from Role and Formation of IMI, G_L is $<1\ kT$ for PE systems.

The rate of LD evolution from a CI is then

$$k_L = [2D_{IMI}/l_c^2] \exp(-G_L/kT). \tag{27}$$

P_L is simply the ratio of k_L to k_{RMI},

$$P_L = (k_L/k_{RMI}) = [2D_{IMI}/l_c^2\alpha_1] \exp[(G_{RMI} - G_L)/kT]. \tag{28}$$

For values of r_0 for egg PE, $E = kT/2$, and $G_L = 1\ kT$, P_L is only ~0.004.

Eq. 28 yields only a lower bound to P_L. We assumed that the spherical micelles are initially in contact and have to diffuse apart in the CI, because it is the simplest assumption. However, during IMI-IMI coalescence, when the walls of the inter-IMI channel first become continuous, the spherical micelles are almost exactly l_c apart. LD formation may be facile at this juncture ($P_L \approx 1$). The true value of P_L is >0.004, but is determined by details of the coalescence mechanism that are experimentally inaccessible.

Rate of LD Elongation

The initial rate at which an LD elongates is limited by the rate of lipid diffusion into the LD. This influx of lipid increases with the length of the center portion of the LD, L. After a short interval of growth, the rate will be limited by the work done against friction in extending the two ends of the LD. We can estimate these LD elongation rates when $-\Delta\mu \ll kT$.

The linear, central portion of the LD is contiguous with the two apposed bilayers along a perimeter $4L$. The flux of lipid across a unit length of this perimeter, J, is (e.g., 47)

$$J = -(ND/kT)(\Delta\mu/\Delta x), \tag{29}$$

where N is the number of lipid molecules per unit area of interface ($= \bar{a}^{-1}$), D is the lipid molecule diffusion coefficient, and x is the distance perpendicular to L in the plane of the bilayer. The lipid chemical potential changes from that of the L_α phase to that of the H_{II} phase over a distance $\Delta x \approx a_0^{1/2}$. Using the dimensions of the H_{II} phase and an initial LD length $a_0^{1/2}$, the initial, lipid diffusion-limited rate of elongation is,

$$dL/dt = (2D/\pi r_h)(a_0/\bar{a})^{3/2}(-\Delta\mu/kT). \tag{30}$$

We have assumed that lipid molecules are incorporated as fast as they can cross the LD perimeter. Molecules need only undergo several lateral displacements to accomodate each new arrival, so this is valid when $Ja^{1/2} \ll \alpha_1$: hence the requirement $(-\Delta\mu/kT) \ll 1$.

The growth described by Eq. 30 is exponential. Eventually, the work done against friction in elongating the LD limits dL/dt. We assume that the frictional work is dominated by the work of moving the two IMI-like terminals of the LD (Fig. 4). We equate the work done against friction in moving one IMI terminal at a velocity dL/dt for an interval dt with the net free energy flux into the LD resulting from accretion of bilayer lipid. This yields

$$dL/dt = (-r_h\Delta\mu)/3\eta(r_0 + l)a_0. \tag{31}$$

η is the viscosity assigned to the bilayer phase (see Eq. 15). Using r_h, a_0, and $\bar{a}$ values for egg PE as before ($\bar{a} = 0.75$ nm^2; 31), $\eta = 1$ poise, and $D = 7 \times 10^{-8}$ cm^{2}s^{-1} (L_α phase phospholipids well above the $L_\beta \rightarrow L_\alpha$ transition; e.g., 42,

43), the initial LD elongation rate is $0.1(-\Delta\mu/kT)$ cm/s, and the limiting rate is $(-2\Delta\mu/kT)$ cm/s. For thermotropic $L_\alpha \rightarrow H_{II}$ transitions, in the neighborhood of T_H, $\Delta\mu$ can be estimated from the enthalpy of the transition, H_H

$$\Delta\mu = H_H(1 - T/T_H). \quad (32)$$

The enthalpy of the egg PE transition is 0.5 kT at $T_H \simeq$ 30°C (34). At a temperature $T = T_H + 1$°K, $-\Delta\mu/kT =$ 0.0017. The initial dL/dt is almost 2 μm/s (incorporation of almost 5×10^4 lipids/s) and the final rate is more than 30 μm/s ($\sim 10^6$ lipids/s). It can be shown that the limiting dL/dt is attained <1 ms after LD formation, when the LD is <10 nm long.

Assembly of LD or RMI into H_{II} Tube Arrays

If either two LD or two RMI are apposed side-to-side within the plane of the original bilayers, an H_{II} channel will be formed between them (Fig. 5). RMI and LD align in this fashion spontaneously. In general, $2r_0 + 2l$ and $2r_s + 2l$ will not be equal to the equilibrium interlamellar spacing in the L_α phase, d_{eq}. Interlamellar forces tend to maintain the spacing, d, at d_{eq}, and will segregate and align the RMI or LD in the manner of Fig. 5 since this minimizes the area of bilayer array over which $d \neq d_{eq}$. Micrographs in reference 23 show this process underway.

LD elongation drives the same process much more rapidly. LD elongate by sweeping up lipid from the contiguous L_α interfaces. As the lipid in the monolayers between two LD (or an LD and RMI) is swept up into the LD, conservation of mass requires that the two structures must be drawn together. This spontaneous segregation strongly affects the H_{II} phase formation rate. Without it, LD and RMI would have random orientations within the planes of the bilayer stacks, presenting barriers to free diffusion (coalescence) of IMI, and leading to very slow alignment of LD and RMI via diffusion during the transition.

Rate of $L_\alpha \rightarrow H_{II}$ Transitions

It is possible to make order-of-magnitude estimates of the time necessary to complete the $L_\alpha \rightarrow H_{II}$ phase transition under certain circumstances. We will do this for transitions via RMI alone and via both RMI and LD, and compare the predicted times with observations. This will show which pathways are likely to exist in real systems. We will calculate as the transition time the time after a temperature jump to $T = T_H + 1$°K required to incorporate all L_α lipid into H_{II}-like structures (LD and RMI). Equations can also be derived for linear increases in temperature with time (D. P. Siegel, unpublished work). We assume that water transport within the L_α phase is fast with respect to the transition time scale.

The transition occurs in three stages. At time $t = 0$, the temperature of the system is instantaneously increased from a temperature less than T_H to a temperature $T = T_H + 1$°K. First, IMI form between apposed bilayers. n_I increases rapidly to a steady-state value n_I^0 (Eq. 13) determined by the competition of IMI production and reversion. The second stage commences when n_I is equal to n_I^0.

The second stage, RMI and LD production, controls the kinetics of the transition. The rate of IMI coalescence is sensitive to the value of n_I^0. If n_I^0 is small, this stage is slow. A small percentage of the lipid of the system exists in IMI at any time. IMI slowly coalesce, forming RMI and LD. When n_I^0 is large, this second stage is rapid and both RMI and LD form quickly. The third stage begins when the rate of lipid incorporation into LD surpasses the rate of lipid addition to RMI via IMI coalescence. The duration of the second stage is therefore also affected by the LD production probability (P_L). If the value of P_L is the lower bound value (Eq. 28), the rate of lipid incorporation into LD exceeds that into RMI after a long period of IMI coalescence. If P_L is large, LD dominate the incorporation rate from the start and the overall rate is much more rapid. The duration of the third stage is also controlled by the LD elongation rate dL/dt, which is sensitive to the ambient temperature (Eqs. 31, 32).

Simple expressions can be derived for the transition time if we make four simplifying assumptions. First, we assume that the number of IMI per unit area of bilayer-bilayer interface, $n_I(t)$, is the steady-state value n_I^0 for $t > 1/C$ (Eq. 13). Second, we assume that the area of apposed bilayer-bilayer interface in the system is constant in time during the transition. Third, we neglect the relatively infrequent coalescence of IMI with pre-existing RMI. Fourth, we assume that dL/dt is constant and is the friction-limited value (Eq. 31).

The first assumption is valid if the rate of IMI production N_3 is larger than the rate of IMI coalescence, $k_I(n_I^0)^2$. This is true: N_3 (3) falls in the range 10^{11}–10^{15} IMI/cm^2/s. We will show below that n_I^0 is the range 10^{10}–10^{11} IMI/cm^2 and k_I is $\sim 10^{-11}$ cm^2/s, so that of $k_I(n_I^0)^2$ is $\sim 10^9$–10^{11}/cm^2/s. Solution of Eq. 12 including a term for IMI coalescence shows that $n_I(t)$ will typically be within ~10% of n_I^0 (D. Siegel, unpublished work).

The second assumption is valid because we only seek order-of-magnitude estimates of t_T. The area available for IMI formation decreases as L_α phase lipid enters the H_{II} phase, so that our assumption will slightly underestimate the transition times. Explicit equations can be derived (D. Siegel, unpublished work) showing that an assumption of linear decrease in bilayer area with time during the transition makes only about a factor of two difference in the predicted times when LD and RMI are both assumed to form, so that this assumption is nevertheless valid for our purposes. If only RMI formed, the true transition time would be several multiples of the value calculated below.

The third assumption is valid because RMI will have a smaller diffusion coefficient than IMI, and react slower than IMI. RMI also tend to aggregate into H_{II} bundles

(Fig. 5), making them less available for reaction with IMI. The fourth assumption is valid because dL/dt reaches the friction-limited value within 1 ms after LD formation, and 1 ms is much smaller than the transition times under these conditions. Relaxation of these assumptions produces unwieldy equations that must be solved via numerical methods (D. Siegel, unpublished work).

With these assumptions, for transitions via both RMI and LD, the number of lipid molecules in H_{II}-like structures at time t after the transition begins is

$$N_T = 2Mk_I(n_I^0)^2t + P_LVk_I(n_I^0)^2\int_0^t [t - t']dt', \quad (33)$$

where M is the number of molecules in an IMI that are incorporated into the CI. It can be shown that

$$M \approx 2S/3(a_0\bar{a})^{1/2} + 4\pi r_0^2, \quad (34)$$

where S is given by Eq. 4, and

$$V = (2\pi r_h/a_0)(dL/dt), \quad (35)$$

where (dL/dt) is given by Eq. 31. The transition is complete when $N_T = 2/\bar{a}$, the number of molecules in the original two apposed bilayer interfaces. Evaluating the integral and rearranging yields the total transition time in systems forming both LD and RMI (including the time $1/C$ that it takes for the IMI concentration to build up to n_I^0):

$$t_{LD} = 1/C + \{-2M + [4M^2 + 4VP_L/\bar{a}k_I(n_I^0)^2]^{1/2}\}/VP_L$$
$$\approx [4/\bar{a}VP_Lk_I(n_I^0)^2]^{1/2}. \quad (36)$$

The second, approximate form of Eq. 36 is valid because M is ~200 in systems like pure PEs (3), which is much smaller than the other term inside the brackets, and because $1/C$ is only in the millisecond range (3).

If we assume that the transition only occurs via RMI, the transition should be complete after several multiples of the time t_{RMI};

$$t_{RMI} \approx 1/\bar{a}Mk_I(n_I^0)^2. \quad (37)$$

Numerical Example: Egg-PE Near Room Temperature or DLPE at 20°C

We will estimate t_{LD} and t_{RMI} for PE with x-ray structural parameters of egg PE and DLPE system investigated by Hui and co-workers (23, 24). These systems should be typical of most PEs of biological interest.

We obtain r_h of pure DLPE at 20°C and egg PE from the d_{110} spacing in x-ray diffraction patterns of the H_{II} phase, which is 3.46 nm (24, 48). The typical thickness of an unsaturated PE bilayer (egg PE; see reference 32) is ~3.2 nm, so that $l = 1.6$ nm. Since $d_{11} = r_h + 1$, r_h is 1.86 nm. r_0 is calculated via Eq. 6, and is 1.3 nm. We assume that $r_0 = r_s$ for the sake of simplicity. We assume that $E = kT/2$ (as in reference 3), and estimate $G^{\ddagger} \approx 10kT$. G_{def} is small compared with kT: with $r_s = r_0$, G_{def} as calculated with Eq. 3 is ~0.03 kT, which is negligible. Eq. 17 yields an upper limit of 6 kT for G_H: we assume $G_H = 3\ kT$ in what follows. M is equal to 200, from Eqs. 6 and 34. We use the value for k_I calculated for egg PE IMI coalescence of $7 \times 10^{-12} \approx 10^{-11}$ cm^{-2} s^{-1} (Eq. 16). We use the value of V calculated for egg PE (H_{II} Phase Formation) of 10^6 molecules/s (Eq. 31).

Although G_{app} can be measured in L_α systems, P_a is difficult to estimate. First, there is reason to believe that some part of G_a can be coupled into G_{mic}: close apposition can raise the local lipid chemical potential of the L_α phase, which should reduce the activation energy necessary to form the IMI. Second, measurements of the interlamellar forces have not been made in systems close to T_H. The head groups of lipids become less hydrated upon adoption of the H_{II} phase, and close apposition of bilayers may become more facile in the vicinity of the $L_\alpha \rightarrow H_{II}$ transition. Hui et al (23) observed that systems exhibiting the most facile ("direct") $L_\alpha \rightarrow H_{II}$ transitions were those in which the L_α lamellar repeat distance decreased with increasing temperature near T_H, implying a weakening of repulsive hydration forces. P_r is hard to estimate for similar reasons.

Accordingly, we assume a range of P_r/P_a values. More work has to be done against hydration forces to appose bilayer interfaces of the critical area A than must be done to flatten an IMI for reversion (H_{II} Phase Formation), so it is hard to imagine P_r/P_a being smaller than unity. A more likely value is e^5, arrived at as follows. About 10 kT is required to appose two 30-nm diameter PE vesicles to within <1 nm near room temperature (35). Making the conservative assumption that this is G_{app} for formation of an IMI in a multilamellar array, $P_a = e^{-10}$ (Eq. 1). We arbitrarily assume that half this energy is required to deform IMI sufficiently for reversion to begin, so that $P_r/P_a = e(-5 + 10) = e^{-5}$.

For this range of values,

$$n_I^0 = 6 \times 10^9 \text{ to } 5 \times 10^{11} \approx 10^{10} - 10^{11} \text{ IMI cm}^{-2}.$$

This is the range we will use in the calculations. Note that this is also the range of "lipidic particle" densities (10^2–10^3 μm^{-2}) observed via rapid-freezing freeze-fracture electron microscopy of lipid samples near the $L_\alpha \rightarrow H_{II}$ phase transition (e.g., 49). If anything, n_I^0 is larger than the morphological results imply, since the fast-freezing time scale (1–10 ms) is on the same order as IMI reversion half-lives (Eq. 10; 3). These values yield the following $L_\alpha \rightarrow H_{II}$ phase transition times when the temperature of the PE L_α phase is instantaneously increased to $T_H + 1°$ K:

$$t_{LD} \approx 1\text{–}10 \text{ s} \quad (P_L = \text{lower bound of } 0.004)$$
$$\approx 0.1\text{–}1 \text{ s} \quad (P_L = \text{upper bound of } 1)$$
$$t_{RMI} \approx 10\text{–}10^2 \text{ s}. \quad (38)$$

Note that t_{LD} is much greater than 1 ms, so that our assumption that the LD elongate at the constant, friction-limited velocity is valid.

The Importance of LD

Only a few time-resolved x-ray diffraction studies of the $L_\alpha \rightarrow H_{II}$ phase transition have been performed. However, all these transition time measurements are much more compatible with the transition times calculated assuming participation of LD than those calculated assuming only RMI formation. The observed transition times are a couple of seconds or less for bacterial PEs (50) and ether analogues of saturated-acyl chain PEs (51) subjected to rapid T-jumps and 0.3–0.4 s for egg PE subjected to a temperature increase rate of ~6°K/s (P. Laggner, manuscript in preparation). The times observed in these experiments may also include delays due to water transport between the two phases (see below) and the transition times of sucessive sub-populations of lipids. It is therefore unlikely that $L_\alpha \rightarrow H_{II}$ transitions in these systems proceed only by RMI, which was the original mechanistic proposal (25, 26). Some sort of LD-like intermediate must exist in order for the transition to proceed on the observed time scales.

LD exert such a powerful influence on the transition rate because they are the fastest path between the L_α and H_{II} phases. The average time between IMI coalescence events per RMI is kn_I^0, or ~0.1–1 s^{-1}. For RMI-mediated transitions the rate of incorporation of molecules into the H_{II} phase per RMI is

$$dN_T/dt = Mk_I n_I^0 \approx 10\text{–}10^2 \text{ lipids/s}, \qquad (39)$$

while the rate of incorporation per LD at $T = T_H + 1$°K is 10^6 lipids/s, or 10^4 times faster than the co-existing RMI pathway. Thus, even if the proportion of IMI-IMI coalescence events that form LD, P_L, is quite small, LD still dominate the kinetics of the transition.

LD-mediated transitions should also create long-range H_{II} phase order much faster than RMI-dominated systems. Micrographs of the H_{II} phase often show images of uninterrupted H_{II} tubes many microns in length. The number of IMI coalescence events per RMI during the $L_\alpha \rightarrow H_{II}$ transition is on the order of $k_I n_I^0 t_{LD}$, which is on the order of unity. These RMI are each the products of only a few IMI-IMI coalescence events, and will be <0.1 μm long. They would have to fuse end-on into long H_{II} tubes after the RMI aligned into bundles (Fig. 5). This takes additional time, so that we should expect to see shorter H_{II} tubes in micrographs of systems rapidly quenched during the transition. In contrast, LD elongate at $dL/dt \approx 30$ μm/s (Eq. 31) even when the system is very weakly superheated ($T = T_H + 1$°K). LD lengths will be about $(dL/dt)t_{LD}$ long, which is microns to hundreds of microns. Thus, LD automatically produce long, aligned H_{II} tubes on the time scale t_{LD}, as is observed, whereas RMI probably cannot.

LD may be difficult to image via freeze-fracture electron microscopy. The number of RMI structures incorporated into the H_{II} phase at the end of the IMI coalescence stage is of order 10^{-1}–1 times n_I^0. The number of LD should be a factor of P_L smaller, so that there will be more RMI than LD in samples quenched during the $L_\alpha \rightarrow H_{II}$ transition if P_L is small. If P_L is close to unity, both the $L_\alpha \rightarrow H_{II}$ and $H_{II} \rightarrow L_\alpha$ transitions can occur on the rapid-freezing time scale, and imaging of any intermediates will be difficult (see "$H_{II} \rightarrow L_\alpha$ Transitions," below). Rapid-freezing will result in a transient temperature jump far below T_H. This will cause LD to contract with a velocity of the same magnitude as given by Eqs. 31 and 32 with $T < T_H$. V will be so large that LD may contract and disappear in 10 ms or less ($n_I^0 = 10^{11}$ cm^{-2}, $P_L = 1$, $T - T_H = -30$°K).

n_I^0 and the $L_\alpha \rightarrow H_{II}$ Transition Rate Are Anti-Correlated With IMI Lifetime

It is obvious from Eqs. 36 and 37 that the rate of the $L_\alpha \rightarrow H_{II}$ transition is sensitive to n_I^0. Factors that increase n_I^0 (e.g., large P_a, decrease in A through a decrease in r_0; Eqs. 6, 8, 13) decrease the transition time. Note that reductions in P_a generally correspond to reductions in P_r, and that reductions in r_0 reduce $G_-^\ddagger$ (Eqs. 2, 11). Thus, factors that increase n_I^0 (Eq. 13) generally decrease both t_{LD} and the half-life of IMI (Eq. 10). The most rapid $L_\alpha \rightarrow H_{II}$ transitions should occur in systems with the most labile IMI. This is consistent with the predictions in reference 3 and with the absence of IMI morphology in freeze-fracture electron micrographs of systems with rapid transitions (23, 24, 25).

For example, in mixtures of dilinoleoyl-PE and palmitoyloleoyl-PC, r_h (and therefore r_0) increases as the mole fraction of PC increases (24). Increases in r_0 should increase A, and increases in the mole fraction of PC should decrease P_a, because of the stronger short-range forces in PC vs. PE systems (30). We therefore expect the lability of IMI to decrease with increasing mole fraction of PC. This should make IMI observable on the ^{31}P-NMR and freeze-fracture electron microscopy time scales (3), whereas $t_{1/2}$ is too short (0.1–1 ms) in pure PE (3). This is as observed. IMI are not observed in the pure PE system (23, 24), but IMI morphology appears as PC content increases (24). The rate of the transition decreases as well, at least in the sense that hysteresis in the transition increases and IMI morphology is observed over a wider temperature range (23, 24). This happens in other PE-PC systems as well (49, 52–54).

Hysteresis in the $L_\alpha \rightarrow H_{II}$ Phase Transition Due to Water Transport

The H_{II} and L_α phases in equilibrium at a given temperature may contain different amounts of water. For instance, the water content of the egg PE H_{II} phase around the

transition temperature is >20% by weight (45), while the content of the L_α phase is closer to 40% (31). In order for multilamellar samples of lipid to adopt the H_{II} phase, a substantial amount of water may have to be transported both within the stacks of lamellae and across the bilayers, which are poorly permeable to water. Lag times due to water transport can delay and broaden the transition, and delay it to different extents when the temperature is raised through T_H at different rates. This may explain the temperature scan rate-dependent thermal hysteresis observed by Yager and Chang in egg PE samples (55). The findings of Ranck et al. (50) are also consistent with this interpretation: the $L_\alpha \leftrightarrow H_{II}$ transition times they report are largest for systems with the greatest differences in structural parameters between the two phases. Usually, the greater this difference, the greater the differences in water content of the phases. The longest relaxation time for $H_{II} \rightarrow L_\alpha$ transitions observed in (50) was several seconds.

The transition times calculated in this paper assume that water transport is fast compared to the transition rate. This will be appropriate when H_{II} phase forms between apposed unilamellar vesicles (22), in permeabilized multilamellar arrays or, perhaps, in oligolamellar systems.

$H_{II} \rightarrow L$ Phase Transitions

The $H_{II} \rightarrow L_\alpha$ transition should occur via the same two paths as the $L_\alpha \rightarrow H_{II}$ transition. The ends of H_{II} tubes are either LD or RMI terminals, and the H_{II} tubes can shorten by LD contraction (lipid molecules diffusing from the walls of H_{II} tubes directly into adjoining bilayer interface) or by RMI fission into IMI. IMI subsequently revert to patches of L_α phase bilayer.

The $H_{II} \rightarrow L_\alpha$ transition may be more hysteretic than the $L_\alpha \rightarrow H_{II}$ transition, since water transport in the H_{II} phase is probably slower than in the L_α phase: transport is essentially one-dimensional (through the center of H_{II} rods) instead of two-dimensional (within aqueous interbilayer slabs). This may explain the greater temperature hysteresis observed via calorimetry in the $H_{II} \rightarrow L_\alpha$ vs. the $L_\alpha \rightarrow H_{II}$ transitions in several PE systems (44, 55).

When the H_{II} phase is formed, most of the molecules enter it via LD, and reside in LD-terminated H_{II} tubes. This is due to the much greater velocity of the LD- vs. RMI-mediated pathway. When the system is subsequently driven through the $H_{II} \rightarrow L_\alpha$ transition, these LD will simply shrink in length (the reverse of the elongation process) with the same velocity given by Eq. 31. Therefore, the time necessary to complete the $H_{II} \rightarrow L_\alpha$ transition should be about the same as t_{LD}.

Some of the H_{II} lipid will exist in structures built up from RMI. The rate of evolution of IMI from the ends of CI should be on the same order of magnitude as the rate of IMI coalescence with pre-existing RMI. The activation energy for evolution of a spherical micelle from a rod micelle is higher than the activation energy of the reverse reaction by an amount G_H (estimated in H_{II} Phase Formation). However, during the $H_{II} \rightarrow L_\alpha$ transition, IMI will be rapidly consumed via reversion to patches of apposed bilayers, and mass action will drive IMI production from RMI.

Are LD Stable Within the Bulk H_{II} Phase?

When the $L_\alpha \rightarrow H_{II}$ transition is complete, a small number of IMI-like terminals of LD will be packed within arrays of H_{II} tubes. It can be shown that the average length between LD terminals in a given H_{II} tube will be on the order of $\bar{a}Vt_{LD}/2(r_h + 1)$, which is tens of microns for PE systems. Moreover, the terminals will not be very mobile within the H_{II} phase: the central portion of an LD cannot expand when all the L_α lipid has been consumed, and contraction requires growth of L_α-like regions at the expense of H_{II} region, which is clearly disfavored. Therefore, it is very unlikely that two terminals will encounter one another and coalesce like two IMI. The LD terminals are probably very long-lived.

It is possible that isolated LD terminals rearrange into other sorts of defects over long periods of time. These other defects may not be able to participate in an $H_{II} \rightarrow L_\alpha$ transition: an LD can contract and transfer lipid to the L_α phase if the lipid-water interfaces of two adjacent H_{II} water channels are continuous around the periphery of the LD terminal. That continuity may be lost if an LD forms another type of defect. If a large fraction of LD terminals rearrange, the $H_{II} \rightarrow L_\alpha$ transition might be much longer than t_{LD}. Since $L_\alpha \rightarrow H_{II}$ and $H_{II} \rightarrow L_\alpha$ phase transition times are about the same under similar conditions (56, 58) we presume that either LD are fairly stable or that LD are rapidly regenerated from other structures during the initial phase of the $H_{II} \rightarrow L_\alpha$ transition.

DISCUSSION

The transition mechanism assumed in this paper involves only structures for which there is morphological evidence. The estimated rates and transition times lead us to several conclusions.

First, transitions via the first proposed mechanism of H_{II} assembly, successive coalescence of IMI into rod micellar structures (25), can only occur in tens or hundreds of seconds. However, $L_\alpha \leftrightarrow H_{II}$ transitions are observed to occur in seconds or less for small T-jumps (50, 51, P. Laggner, manuscript in preparation). Moreover, times measured in experiments like those in (49) are the total of the time delay due to water transport within the phases and the transition times of successive subpopulations of lipid. There are reports that some $H_{II} \rightarrow L_\alpha$ transitions are much faster (1). Transitions via the mechanism in (25) are very unlikely to be this rapid.

Second, the line defect (LD) structures I propose here should form in significant numbers from IMI-IMI coalescence events as secondary intermediates. Once formed, they provide a very rapid pathway between the L_α and H_{II}

phases, and dominate the transition kinetics. Structures of similar morphology have been observed via electron microscopy (1, 23, 25). The kinetic analysis shows that even if LD form infrequently ($P_L \ll 1$), they substantially reduce $L_\alpha \leftrightarrow H_{II}$ transition times. In the limit $P_L \rightarrow$ unity (which is possible in the current model), transition times could be tens-hundreds of milliseconds. Transitions driven by large temperature jumps, for which $-\Delta\mu$ and V are large (Eqs. 31, 32), could occur in the millisecond regime. These conditions are encountered during rapid freezing of H_{II} samples for electron microscopy, and may explain the difficulty in imaging transition intermediates by this technique in some PE preparations (1): the transition runs on the same time scale as the freezing process. The freeze-fracture morphology of nascent H_{II} phase is also more easily rationalized in terms of LD-dominated, as compared to RMI-dominated, transitions. LD can assemble into the observed aligned, multi-micron lengths of H_{II} tubes in times of 1 s or less, while RMI require much longer to do so.

Third, the rate of $L_\alpha \leftrightarrow H_{II}$ transitions is also sensitive to the steady-state number of IMI that form per unit area of bilayer-bilayer interface, n_I^0. n_I^0 cannot be accurately calculated, but should be in the range 10^{10}–$10^{11}/cm^2$ (consistent with the range of concentrations of "lipidic particles" observed via freeze-fracture electron microscopy; see reference 3). Factors that increase n_I^0 (smaller r_h, increased ease of close apposition, smaller mole fractions of lamellar-phase impurities) should shorten transition times. The same factors that increase n_I^0 shorten the half-life of IMI with respect to reversion. Thus, systems with the fastest transitions have the most labile IMI. In such cases, IMI half-lives may be in the sub-millisecond regime (3), consistent with the absence of isotropic ^{31}P-NMR resonances and "lipidic particle" morphology in pure PE systems.

Much of the hysteresis in $L_\alpha \leftrightarrow H_{II}$ phases may be due to differences in water content of the phases at equilibrium and the sluggishness of water transport within them. Similar suggestions have been made by others (30, 50). In deriving the kinetic estimates, I assumed that either water transport was rapid on the transition time scale or that the difference in water contents between the equilibrium phases was trivial. Often, this will not be the case. Observed transition times in multilamellar, oligolamellar, permeabilized multilamellar, and aggregated unilamellar dispersions may be different on this account.

Finally, some corrections were made to the IMI formation rate and n_I^0 expressions derived in reference 3. IMI should not revert to patches of apposed bilayers and inter-bilayer attachments (ILA, Fig. 1 *d*, right) with equal frequency, as assumed in reference 3. ILA should form rarely in pure PE. This has important consequences for the behavior of vesicle dispersions and the structure of some inverted cubic phases (23, 24), and will be discussed in (22) and a manuscript in preparation, respectively.

Other mechanisms for these transitions have been proposed. The intermediates proposed to participate in some models seem unlikely on kinetic grounds.

Line Defect Structures Are Secondary Intermediates in $L_\alpha \rightarrow H_{II}$ Transitions

In this model, IMI represent the first loci at which the lipid-water interfaces of apposed bilayers become continuous. This is consistent with observations that unilamellar vesicle suspensions do not show morphological evidence of the phase transition when H_{II} is the equilibrium phase until the vesicles aggregate (56, 57). The interfaces of apposed lipid bilayers must become continuous in order for the $L_\alpha \rightarrow H_{II}$ transition to occur: in reference 3 I showed that the formation of inverted micellar intermediates and H_{II} rods within isolated bilayers was exceedingly unlikely, and that the transition had to be an interbilayer phenomenon in order to occur on a time scale shorter than days.

It has been suggested that linear confluences of apposed bilayer-water interfaces tens of nm or more long are the first structures to form during this transition (1, 23, 24). It is obvious that apposed bilayers are more likely to first become continuous around the perimeter of objects the size of IMI. The activation energy required to make two lipid-water interfaces continuous must grow at least linearly with the perimeter of the initial connection. Work must be done against short-range repulsive forces (31–33) to closely-appose the interfaces, and some energy must be spent in disrupting lipid-lipid interactions in the planes of the two interfaces. Both these contributions increase with the area of interface apposed and can each be significant compared to kT per lipid molecule, so that the activation energy increases rapidly with increasing perimeter of the first membrane-membrane continuity. Assuming an Arrhenius-type formation rate, this means that the formation rate decreases exponentially with increasing perimeter length. IMI, with an initial continuity perimeter of ~3 nm for PE (3), form orders of magnitude faster than line defects tens of nm long. Line defects like those proposed in (1, 23, 24) are therefore very unlikely to be the first structures that form during the transition.

The LD intermediates I propose here are consistent with the morphology cited in references 1, 23 and 24 and can form readily from the first intermediates, IMI. In this fashion, the system assembles the H_{II} phase from many low-activation energy structures (IMI), as opposed to formation of fewer but much higher activation energy (hence, improbable) structures. The same principle suggests that smaller primary intermediates than IMI should form. I will now show that the free energy of curvature of the lipid-water interfaces in such structures is too unfavorable for them to form in significant numbers.

"Conical LIP"-Like Structures are Unlikely

In their careful study of the $L_\alpha \rightarrow H_{II}$ and C_{II} transitions in PE-PC mixtures, Hui et al. (23) observed freeze-fracture

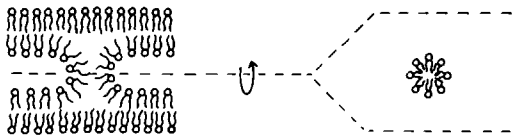

FIGURE 6 Conical LIP structure, as described in reference 23. *Left*: cross-section in the plane perpendicular to the apposed bilayers. *Right*: cross section in the plane parallel to and equidistant from two apposed bilayers.

morphology they interpreted in terms of a "conical LIP" structure. This structure is depicted in Fig. 6: the connection between the two bilayers has the same exterior shape as an IMI, but there is no micelle enclosed by the exterior monolayer. If such structures form, they could elongate rapidly into LD, the play a role in the $L_\alpha \rightarrow H_{II}$ phase transition.

However, this structure seems unlikely: the curvature energy, and hence the activation energy for formation of this structure, is very large. The positive radius of curvature in the plane between the bilayers is equal to the monolayer thickness. This is the length of a lipid molecule, and is approximately one-third the corresponding radius in IMI. Such a radius of curvature means that several methylene groups of the acyl chains of each lipid molecule are exposed to water. Eq. 4 predicts a curvature free energy of $\sim 100\ kT$ for such a structure, using r_h and l data appropriate for PE at 20°C (23, 24, 31) and $k_c = 10^{-12}$ erg. Moreover, expressions like Eq. 4 should break down and yield underestimates when both radii of curvature are on the order of molecular dimensions, as with this case. The total free energy of activation for formation of a conical LIP will be greater than the curvature free energy, and a (rare) concentration fluctuation in the apposed bilayers may be required to form it, as described in reference 3. The large activation energy results in a trivial formation rate for such structures ($<10^{-1}$/cm^2/s for an activation energy of 50 kT, frequency factor α_1, and cross-sectional diameter of $2[r_h + 1]$). We therefore expect that conical LIP-type structures are very rare, if they form at all.

Complex Hexagonal Intermediates in the $L_\alpha \rightarrow H_{II}$ Transition

Borovjagin et al. reported (28) that the $L_\alpha \rightarrow H_{II}$ transition in mixtures of egg PC and cardiolipin (EPC-CL) involved formation of complex hexagonal phase structures. These are cylindrical tubes of bilayers, the interior water channel having the same radius as the water channel in the H_{II} phase. This conclusion was based on thin-section negative-stain electron microscopy and the observation of two tube thicknesses in freeze-fracture electron micrographs of the nascent H_{II} phase, the thicker tubes being compatible with complex hexagonal tube dimensions.

There are five problems with this interpretation. First, these two classes of tube diameters have been observed previously in similar systems, occasionally apposed side-by-side (25). If the larger variety of tubes are bilayer cylinders, this would mean that the head groups on the exterior surface of the complex hexagonal tube are apposed to ends of the acyl chains of lipids on the normal H_{II} tube: this is highly unlikely. Van Venetie and Verkleij (25) suggest that this dichotomy represents a partial lateral phase separation of the two lipid components, resulting in larger water channel diameters for the PC-rich mixture.

Second, the complex hexagonal structure has a high curvature energy compared to RMI and IMI. The curvature free energy of a length L of the bilayer when the equilibrium radius is r_h (H_{II} phase) is

$$G' = 2\pi RLk_c(1/R + 1/r_h)^2, \qquad (40)$$

where R is the diameter of the complex hexagonal tube. For R values observed in reference 28 of ~6 nm, $L = 2r_h$ (to make the surface area roughly comparable to IMI), r_h = ~1 nm (28), and an optimistically low $k_c = 10^{-13}$ erg, we find that G'' is ~250 kT. This is a very large energy, which makes this structure very unlikely (particularly when lengths much larger than $2r_h$ are observed; [25, 28]).

Third, it is not clear how the complex hexagonal phase would form. This process is depicted (Fig. 10 E and 10 E' of reference 28) as involving the simultaneous fission of two apposed bilayers. This would be a much higher activation-energy and rarer process than the fusion of apposed monolayers, as in IMI formation. Fourth, it is not clear how complex hexagonal structures would shed their outermost monolayers to become H_{II} arrays at a significant rate, as Borovjagin et al. pointed out (28). Fifth, the identification of the thick tubes as the complex hexagonal phase was made on the basis of thin-section negative stain electron microscopy in reference 28. The samples were prepared by ethanol series dehydration after exposure to glutaraldehyde-tannic acid, osmium tetroxide, and uranyl acetate. This procedure might result in morphology unrepresentative of the initial state of the system.

Therefore, we assume that complex hexagonal structures are not intermediates in the $L_\alpha \rightarrow H_{II}$ transition. We also note that many features visible in Figs. 3–7 of reference 27 are compatible with RMI and LD morphology.

$L_\alpha \rightarrow H_{II}$ Transitions Driven By Divalent Cation Binding

The expressions in this paper are derived for thermotropic $L_\alpha \leftrightarrow H_{II}$ transitions. The transition in some systems is driven by divalent cation binding to anionic lipid. For example, at room temperature and neutral pH, bovine heart cardiolipin adopts the H_{II} phase in the presence of divalent cations such as Ca^{2+} or Mg^{2+} (58, 59). The methods used here to estimate transition times are inapplicable in those cases. The chemical potential and equilibrium curvature of lipid-water interfaces are sensitive functions of the local divalent cation concentration. For

example, the enthalpy of Ca^{2+} binding in the Ca^{2+}-cardiolipin system increases from ~200 cal/mole to 1,800 cal/mole as the Ca^{2+}-to-cardiolipin mole ratio is increased from 0.5 to 17 (59). The equilibrium curvature in the H_{II} phase also depends on $[Ca^{2+}]$ (58). This means that at a given local $[Ca^{2+}]$, the chemical potential differences between lipid aggregates with different radii of curvature can be much larger than for thermotropic $L_\alpha \rightarrow H_{II}$ transitions. This greatly affects the activation energies for formation and reversion of IMI, IMI coalescence, etc. Severe hysteresis as a function of $[Ca^{2+}]$ can also occur (59; see discussion in reference 3). The rates of the individual steps in the transition will therefore be different than predicted by the present theory, which is only a qualitative description of $L_\alpha \rightarrow H_{II}$ transitions of this type.

Implications for Time-Resolved X-Ray Diffraction Studies

Some rough conclusions can be drawn concerning the populations of lipid in different structures during the transition and the likely diffraction patterns. The first structures to form are IMI. The fraction of the lipid in IMI at any time is probably small, and decreases with time as lipid enters the H_{II} phase. The maximum fraction of lipid in IMI, f_{IMI}, is

$$f_{IMI} \approx (\bar{a})\mathrm{Mn}_l^0, \tag{41}$$

which is in the range 1–10%. f_{IMI} decreases with a relaxation time $\approx t_{LD}$. IMI are also small (~10 nm-diameter) structures that will be irregularly spaced in most systems. This implies that they will not produce well-defined features in the instantaneous diffraction pattern of the lipid system, and that the intensity of any such features will be weak.

The next structures to form are RMI and LD, which closely resemble H_{II} tubes. Therefore, we do not expect these structures to result in novel features in the instantaneous x-ray diffraction pattern, either. The diffraction pattern should simply resemble a superposition of the L_α and H_{II} patterns, the relative amplitude of the two components changing with time. The lines arising from the H_{II} phase will probably become narrower in the second or so following disappearance of the L_α lines, since RMI will be fusing into longer H_{II} tubes, which will be more tightly and regularly packed. There may be a diffuse, low-intensity signal from IMI in some systems. These expectations are compatible with observations to data (50, 51).

The author is grateful to S. W. Hui, Greg Kirk, and Sol Gruner for useful discussions, to D. F. Hager for helpful discussions and for help in editing manuscript, to Ms. Michaelle Jones for numerical integration of some expressions, and to Isao Noda for advice on solution of an integral differential equation.

Received for publication 3 April 1985 and in final form 17 January 1986.

REFERENCES

1. Verkleij, A. J. 1984. Lipidic intramembranous particles. *Biochim. Biophys. Acta.* 779:43–63.
2. Cullis, P. R., B. de Kruijff, M. J. Hope, A. J. Verkleij, R. Nayar, S. B. Farren, C. Tilcock, T. D. Madden, and M. B. Bally. 1983. Structural properties of lipids and their functional roles in biological membranes. *In* Membrane Fluidity in Biology. Vol. 1. Academic Press, Inc., New York. 39–81.
3. Siegel, D. P. 1984. Inverted micellar structures in bilayer membranes: formation rates and half-lives. *Biophys. J.* 45:399–420.
4. Nayar, R., M. J. Hope, and P. R. Cullis. 1982. Phospholipids as adjuncts for calcium ion-stimulated release of chromaffin granule contents: implications for mechanisms of exocytosis. *Biochemistry.* 21:4583–4589.
5. Quinn, P. J., and W. P. Williams. 1983. The structural role of lipids in photosynthetic membranes. *Biochim. Biophys. Acta.* 737:223–266.
6. Gruner, S. M., K. J. Rothschild, and N. A. Clark. 1982. X-ray diffraction and electron microscope study of phase separation in rod outer segment photoreceptor membrane multilayers. *Biophys. J.* 39:241–251.
7. Albert, A. D., A. Sen, and P. L. Yeagle. 1984. The effect of calcium on the bilayer stability of lipids from bovine outer rod segment disk membranes. *Biochim. Biophys. Acta.* 771:28–34.
8. Crowe, L. M., and J. H. Crowe. 1982. Hydration-dependent hexagonal phase lipid in a biological membrane. *Arch. Biochem. Biophys.* 217:582–587.
9. Van Venetie, R., and A. J. Verkleij. 1982. Possible role of non-bilayer lipids in the structure of mitochondria: a freeze-fracture electron microscopy study. *Biochim. Biophys. Acta.* 692:397–405.
10. Hope, M. J., and P. R. Cullis. 1979. The bilayer stability of inner monolayer lipids from the human erythrocyte. *FEBS (Fed. Eur. Biochem. Soc.) Lett.* 107:323–326.
11. Kirk, G. L., S. M. Gruner, and D. L. Stein. 1984. A thermodynamic model of the lamellar to inverse hexagonal phase transition of lipid membrane-water systems. *Biochemistry.* 23:1093–1102.
12. Ellens, H., J. Bentz, and F. C. Szoka. 1984. pH-induced destabilization of phosphatidylethanolamine-containing liposomes: role of bilayer contact. *Biochemistry.* 23:1532–1538.
13. Sundler, R., N. Duzgunes, and D. Papahadjopoulos. 1981. Control of membrane fusion by phospholipid head groups. II. The role of phosphatidylethanolamine in mixtures with phosphatidate and phosphatidylinositol. *Biochim. Biophys. Acta.* 649:751–758.
14. Duzgunes, N., J. Wilschut, R. Fraley, and D. Papahadjopoulos. 1981. Studies on the mechanism of membrane fusion: role of head group composition in calcium- and magnesium-induced fusion of mixed phospholipid vesicles. *Biochim. Biophys. Acta.* 642:182–195.
15. Kolber, M. A., and D. H. Haynes. 1979. Evidence for a role of phosphatidylethanolamine as a modulator of membrane-membrane contact. *J. Membr. Biol.* 48:95–114.
16. Wilschut, J., M. Holsappel, and R. Jansen. 1982. Ca^{2+}-induced fusion of cardiolipin/phosphatidylcholine vesicles monitored by mixing of aqueous contents. *Biochim. Biophys. Acta.* 690:297–301.
17. Taraschi, T. F., A. T. M. van der Steen, B. de Kruijff, C. Tellier, and A. J. Verkleij. 1982. Lectin-receptor interactions in liposomes: evidence that binding of wheat germ agglutinin to glycoprotein-phosphatidylethanolamine vesicles induces non-bilayer structures. *Biochemistry.* 21:5756–5764.
18. de Kruijff, B., and P. R. Cullis. 1980. Cytochrome c specifically induces nonbilayer structures in cardiolipin-containing model membranes. *Biochim. Biophys. Acta.* 602:477–490.
19. Yau, L. Y., and S. I. Chan. 1975. Alamethicin-mediated fusion of lecithin vesicles. *Proc. Natl. Acad. Sci. USA.* 72:2170–2174.
20. Hah, J.-S., S. W. Hui, and C. Y. Jung. 1983. Effects of physical

states of phospholipids on the incorporation and cytochalaisin B binding activity of human erythrocyte membrane proteins in reconstituted vesicles. *Biochemistry.* 22:4763–4769.
21. Jensen, J. W., and J. S. Schutzbach. 1984. Activation of mannosyltransferase II by nonbilayer phospholipids. *Biochemistry.* 23:1115–1119.
22. Siegel, D. P. Inverted micellar intermediates and the transitions between lamellar, cubic, and inverted hexagonal lipid phases. II. Implications for membrane-membrane interactions and membrane fusion *Biophys. J.* 49:1171–1183.
23. Hui, S. W., T. P. Stewart, and L. T. Boni. 1983. The nature of lipidic particles and their roles in polymorphic transitions. *Chem. Phys. Lipids.* 33:113–126.
24. Boni, L. T., and S. W. Hui. 1983. Polymorphic phase behavior of dilinoleoylphosphatidylethanolamine and palmitoyloleoylphosphatidylcholine mixtures: structural changes between hexagonal, cubic, and bilayer phases. *Biochim. Biophys. Acta.* 731:177–185.
25. van Venetie, R., and A. J. Verkleij. 1981. Analysis of the hexagonal II phase and its relations in lipidic particles and the lamellar phase: a freeze-fracture study. *Biochim. Biophys. Acta.* 645:262–269.
26. Verkleij, A. J., C. J. A. van Echteld, W. J. Gerritsen, P. R. Cullis, and B. DeKruijff. 1980. The lipidic particle as an intermediate structure in the membrane fusion process and bilayer to hexagonal (H_{II}) transitions. *Biochim. Biophys. Acta.* 600:620–624.
27. Gounaris, K., A. Sen, A. P. R. Brain, P. J. Quinn, and W. P. Williams. 1983. The formation of non-bilayer structures in total polar lipid extracts of chloroplast membranes. *Biochim. Biophys. Acta.* 728:129–139.
28. Borovjagin, V. L., J. A. Vergara, and T. J. McIntosh. 1982. Morphology of the intermediate stages of the lamellar to hexagonal lipid phase transition. *J. Membr. Biol.* 69:199–212.
29. Cullis, P. R., B. DeKruijff, M. J. Hope, R. Nayar, and L. Schmid. 1980. Phospholipids and membrane transport. *Can. J. Biochem.* 58:1091–1100.
30. Gruner, S. M., K. J. Rothschild, W. J. DeGrip, and N. A. Clark. 1985. Co-existing lyotropic liquid crystals: commensurate, faceted and co-planar single hexagonal (H_{II}) domains in lamellar photoreceptor membranes. *J. Physiol. (Paris).* 46:193–201.
31. Lis, L., M. McAlister, N. Fuller, R. P. Rand, and V. A. Parsegian. 1982. Interactions between neutral phospholipid bilayer membranes. *Biophys. J.* 37:667–672.
32. Rand, R. P. 1981. Interacting phospholipid bilayers: measured forces and induced structural changes. *Annu. Rev. Biophys. Bioeng.* 10:277–314.
33. Cowley, A. C., N. L. Fuller, R. P. Rand, and V. A. Parsegian. 1978. Measurement of repulsive forces between charged phospholipid bilayers. *Biochemistry.* 17:3163, 3168.
34. Hardman, P. D. 1982. Spin-label characterization of the lamellar-to-inverted hexagonal (H_{II}) phase transition in egg-phosphatidylethanolamine. *Eur. J. Biochem.* 124:95–101.
35. Galla, H.-J., W. Hartmann, U. Thielen, and E. Sackmann. 1979. On two-dimensional passive random walk in lipid bilayers and fluid pathways in biomembranes. *J. Membr. Biol.* 48:215–236.
36. Gamble, R. C., and P. R. Schimmel. 1978. Nanosecond relaxation processes of phospholipid bilayers in the transition zone. *Proc. Natl. Acad. Sci. USA.* 75:3011–3014.
37. Helfrich, W. 1973. Elastic properties of lipid bilayers: theory and possible experiments. *Z. Naturforsch.* 28C:693–703.
38. Sakurai, I., and Y. Kawamura. 1983. Magnetic field-induced orientation and bending of myelin figures of phophatidylcholine. *Biochim. Biophys. Acta.* 735:189–192.
39. Servuss, R. M., W. Harbich, and W. Helfrich. 1976. Measurement of the curvature-elastic modulus of egg lecithin bilayers. *Biochim. Biophys. Acta.* 436:900–903.
40. Ninham, B. W., and V. A. Parsegian. 1970. Van der Waals interactions in multilayer systems. *J. Chem. Phys.* 53:3398–3402.
41. Torney, D. C., and H. M. McConnell. 1983. Diffusion-limited reaction rate theory for two-dimensional systems. *Proc. R. Soc. Lond.* A387:147–170.
42. Vaz, W. L. C., M. Criado, V. M. C. Madeira, G. Schoellmann, and T. M. Jovin. 1982. Size dependence of the translational diffusion coefficient of large integral membrane proteins in liquid-crystalline phase lipid bilayers: a study using fluorescence recovery after photobleaching. *Biochemistry.* 21:5608–5612.
43. Peters, R., and R. J. Cherry. 1982. Lateral and rotational diffusion of bacteriorhodopsin in lipid bilayers: experimental test of the Saffman-Delbruck equations. *Proc. Natl. Acad. Sci. USA.* 79:4317–4321.
44. Rand, R. P., and N. L. Fuller. Measured hydration energy of the aqueous cavities of the phospholipid inverted hexagonal phase. 1985. *Biophys. J.* 47 (2, Pt. 2):423*a*. (Abstr.)
45. Reiss-Husson, F. 1967. Structure des phases liquide-crystallines de differents phopholipides, monoglycerides, sphingolipides, anhydres ou en presence d'eau. *J. Mol. Biol.* 25:363–382.
46. W. H. Beyer, editor. 1978. CRC Handbook of Mathematical Sciences. CRC Press, Inc.
47. Tanford, C. 1961. Physical Chemistry of Macromolecules. John Wiley & Sons, NY.
48. van Duijn, G., A. J. Verkleij, and B. de Kruijff. 1984. Influence of phospholipid peroxidation on the phase behavior of phosphatidylcholine and phosphatidylethanolamine aqueous dispersions. *Biochemistry.* 23:4969–4977.
49. Hui, S. W., T. P. Stewart, P. L. Yeagle, and A. D. Albert. 1981. Bilayer to nonbilayer transition in mixtures of phosphatidylethanolamine and phosphatidylcholine: implications for membrane properties. *Arch. Biochem. Biophys.* 207:227–240.
50. Ranck, J. L., L. Letellier, E. Schechter, B. Krop, P. Pernot, and A. Tardieu. 1984. X-ray analysis of the kinetics of E. coli lipid and membrane structural transitions. *Biochemistry.* 23:4955–4961.
51. Caffrey, M. 1985. Kinetics and mechanism of the lamellar gel/lamellar liquid-crystal and lamellar/inverted hexagonal phase transition, in phosphatidylethanolamine: A real-time x-ray diffraction study using synchrotron radiation. *Biochemistry.* 24:4826–4844.
52. Cullis, P. R., and B. de Kruijff. 1978. Polymorphic phase behavior of lipid mixtures as detected by ^{31}P-NMR. *Biochim. Biophys. Acta.* 507:207–218.
53. Cullis, P. R., P. W. M. van Dijck, B. de Kruijff, and J. de Gier. 1978. Effects of cholesterol on the properties of synthetic phosphatidylethanolamine and phosphatidylcholine: a ^{31}P-NMR and differential scanning calorimetry study. *Biochim. Biophys. Acta.* 513:21–30.
54. Tilcock, C. P. S., T. P. Stewart, P. L. Yeagle, and A. D. Albert. 1982. Influence of cholesterol on the structural preferences of dioleoylphophatidylethanolamine-dioleoylphosphatidylcholine systems: a ^{31}P- and ^{2}H-NMR study. *Biochemistry.* 21:4596–4601.
55. Yager, P., and E. L. Chang. 1983. Destabilization of a lipid non-bilayer phase by higher pressure. *Biochim. Biophys. Acta.* 731:491–494.
56. Hui, S. W., and T. P. Stewart. 1981. 'Lipidic particles' are intermembrane attachment sites. *Nature (Lond.).* 290:427–428.
57. Bearer, E. L., N. Duzgunes, D. S. Friend, and D. Papahadjopoulos. 1982. Fusion of phospholipid vesicles arrested by quick-freezing: the question of lipidic particles as intermediates in membrane fusion. *Biochim. Biophys. Acta.* 693:93–98.
58. Rand, R. P., and S. Sengupta. 1972. Cardiolipin forms hexagonal structures with divalent cations. *Biochim. Biophys. Acta.* 255:484–492.
59. de Kruijff, B., A. J. Verkleij, J. Leunissen-Bijvelt, C. J. A. van Echteld, J. Hille, and H. Rijnbout. 1982. Further aspects of the Ca^{2+}-dependent polymorphism of bovine heart cardiolipin. *Biochim. Biophys. Acta.* 693:1–12.